PHYSICAL REVIEW A **96**, 063405 (2017)

Beyond-Born-Oppenheimer effects in sub-kHz-precision photoassociation spectroscopy of ytterbium atoms

Mateusz Borkowski,[1,*] Alexei A. Buchachenko,[2] Roman Ciuryło,[1] Paul S. Julienne,[3] Hirotaka Yamada,[4] Yuu Kikuchi,[4] Kakeru Takahashi,[4] Yosuke Takasu,[4] and Yoshiro Takahashi[4]

[1]*Institute of Physics, Faculty of Physics, Astronomy and Informatics, Nicolaus Copernicus University, Grudziadzka 5, 87-100 Torun, Poland*
[2]*Skolkovo Institute of Science and Technology, 100 Novaya Street, Skolkovo, Moscow Region 143025, Russia*
[3]*Joint Quantum Institute, NIST, and the University of Maryland, College Park, Maryland 20742, USA*
[4]*Department of Physics, Graduate School of Science, Kyoto University, Kyoto 606-8502, Japan*

(Received 23 September 2017; published 6 December 2017)

We present high-resolution two-color photoassociation spectroscopy of Bose-Einstein condensates of ytterbium atoms. The use of narrow Raman resonances and careful examination of systematic shifts enabled us to measure 13 bound-state energies for three isotopologues of the ground-state ytterbium molecule with standard uncertainties of the order of 500 Hz. The atomic interactions are modeled using an *ab initio* based mass-scaled Born-Oppenheimer potential whose long-range van der Waals parameters and total WKB phase are fitted to experimental data. We find that the quality of the fit of this model, of about 112.9 kHz (rms) can be significantly improved by adding the recently calculated beyond-Born-Oppenheimer (BBO) adiabatic corrections [J. J. Lutz and J. M. Hutson, J. Mol. Spectrosc. **330**, 43 (2016)] and by partially treating the nonadiabatic effects using distance-dependent reduced masses. Our BBO interaction model represents the experimental data to within about 30.2 kHz on average, which is 3.7 times better than the "reference" Born-Oppenheimer model. We calculate the s-wave scattering lengths for bosonic isotopic pairs of ytterbium atoms with error bars over two orders of magnitude smaller than previous determinations. For example, the s-wave scattering length for ^{174}Yb is $+5.55812(50)$ nm.

DOI: 10.1103/PhysRevA.96.063405

I. INTRODUCTION

Photoassociation [1,2] is the act of forming a molecule from a pair of colliding atoms through optical excitation. If a laser is tuned to match the difference between the near-zero collision energy and an excited bound state, atom loss is observed. The detuning of the laser from atomic resonance indicates the energy of the molecular vibrational state with respect to its dissociation limit. Photoassociation spectroscopy, first demonstrated for alkali atoms [3–8], was quickly extended to divalent species Ca [9,10], Sr [11–14], Yb [15,16], and Hg [17]. The intercombination lines present in divalent species enable photoassociation spectroscopy to be conducted at high resolution [18]. Two-photon processes are also possible: both Raman [19] and Autler-Townes [20,21] laser configurations can be used to measure the positions of ground-state energy levels in a process known as two-color photoassociation spectroscopy [22–26]. Photoassociation spectroscopy has also been demonstrated for heteronuclear molecules, for example, RbYb [27,28] and LiRb [29]. Due to preferential Franck-Condon factors between the ground scattering state and weakly bound excited states, photoassociation spectroscopy is primarily used for the measurements of bound states close to the appropriate dissociation limit.

Precise measurements of ground-state energy levels near the dissociation limits are immensely important from the point of view of the physics of ultracold collisions. The s-wave scattering length, a fundamental parameter for the physics of Bose-Einstein condensates (BECs) [30], is closely related to the position of the most weakly bound state in a ground-state molecule [31] as they both depend primarily on the long-range van der Waals coefficient C_6 and the total zero-energy WKB phase ϕ of their interaction potential. It is therefore no surprise that the most accurate determinations of scattering lengths for, e.g., Yb [32], Ca [33], or Sr [34] are based on photoassociative investigations of the long-range interactions in their respective dimers. The s-wave scattering lengths play an important role in the density shifts present in optical atomic clocks [35–38]. Precise knowledge of s-wave scattering lengths between ground-state atoms is a prerequisite for the determination of scattering lengths in ground-excited-state and excited-excited-state atomic collisions through measurements of atomic pairs in optical lattices [39,40].

The Born-Oppenheimer approximation plays a central role in molecular physics. It provides us with the notion of an interatomic potential curve. Within this approximation, the atomic interactions are the same regardless of isotopes forming the molecule, which makes it possible to calculate the physical properties, e.g., scattering lengths, for one isotopologue using data from another [31,41]. On the other hand, there are several, generally mass-dependent corrections to this approximation, known together as beyond-Born-Oppenheimer (BBO) effects. The most widely known effect is the diagonal (or adiabatic) Born-Oppenheimer correction (DBOC) [42], which can be seen as a molecular analog of the isotopic mass shift known from atomic spectroscopy. Similarly, additional isotope-dependent interactions stem from the finite nuclear volume [43]. Both corrections have been recently estimated for Yb$_2$ by Lutz and Hutson [44]. Finally, nonadiabatic effects [45–48] can be partially accounted for using the concept of effective reduced masses [49,50].

Interactions between ground- or excited-state ytterbium atoms have been extensively studied using photoassociation experiments. Single-color photoassociation spectroscopy has been utilized to study interactions near the $^1S_0 + {}^1P_1$ [15]

---

[*] mateusz@fizyka.umk.pl

and $^1S_0 + ^3P_1$ [16,51,52] asymptotes. Intercombination line photoassociation spectroscopy has also been used to investigate interisotope Yb_2 molecules [53], as well as exotic subradiant states [54]. Intercombination line photoassociation spectroscopy provides the positions of associated optical Feshbach resonances [55,56], which can be used, as demonstrated in Ref. [57], to effectively control the s-wave scattering lengths.

Two-color photoassociation spectroscopy has been performed previously in thermal samples of Yb atoms and has enabled the determination of scattering lengths in this system [32]. In this work, however, we utilize two-color Raman photoassociation spectroscopy of BECs of ytterbium atoms that is two orders of magnitude more precise than the previous experiment. Instead of a model potential, in this work our interaction model is based on *ab initio* calculations [58] and is further improved by including the BBO effects. Finally we calculate the s-wave scattering lengths for bosonic isotopes of Yb. The paper is organized as follows: a description of the photoassociation experimental setup is found in Sec. II and is followed by the account of systematic shifts in Sec. III. Our interaction models are described in detail in Sec. IV. The fitting of the models and the resulting model parameters and calculated s-wave scattering lengths are discussed in Sec. V. Section VI concludes the paper.

II. PHOTOASSOCIATION SETUP

The lowest-energy levels of the Yb atom are shown in Fig. 1(a). The strong $^1S_0$-$^1P_1$ transition at 399 nm is used for Zeeman slowing. The intercombination $^1S_0$-$^3P_1$ transition at 556 nm is used for laser cooling and photoassociation spectroscopy [16,32]. An additional laser at 532 nm is used to form a far-off resonance trap (FORT). Contrary to our previous determination of the bound-state energies of Yb_2 using two-color photoassociation spectroscopy [32], which utilized thermal atoms, we performed our measurements in BECs of ^{168}Yb, ^{170}Yb, and ^{174}Yb atoms. Typically, 1×10^4 condensate atoms were obtained after evaporative cooling in our FORT and the atom density was around 10^{14} cm^{-3}. The procedures of creating BECs using this setup were previously published for all the investigated isotopes [59–61] and we will only describe the optical setup necessary to perform the two-color photoassociation spectroscopy.

In this experiment, pairs of colliding ground-state atoms are transferred by a Raman process induced by two detuned 556 nm lasers operating near the $^1S_0 \rightarrow ^3P_1$ transition [see Fig. 1(b)] to a bound state in the electronic molecular ground state. We observed the two-color photoassociation (PA) signals by measuring the number of atoms remaining after the irradiation of the PA light by use of the absorption imaging method with the $^1S_0$-$^1P_1$ transition. After the evaporative cooling, two lasers, i.e., L_1 for the free-bound transition and L_2 for the bound-bound transition, were simultaneously applied to the atoms in the FORT for about 30–100 ms. These beams were focused to about an 80 μm diameter.

From symmetry considerations, it follows that two like ground-state bosonic Yb atoms may only collide in even partial waves, $l = 0,2,4,\ldots$. In the $^1S_0 + ^1S_0$ ground state, the total angular momentum $\vec{J} = \vec{l} + \vec{j}$ is, trivially, equal to the rotational angular momentum l because the total electronic angular momentum $j = 0$. At ultracold temperatures, s-wave collisions are dominant. Following the $J = 0 \not\rightarrow J = 0$ selection rule, the first PA photon may only transfer the two s-wave ($J = 0$) atoms to $J = 1$ excited states—in our case, bound states of the $^1S_0 +^3 P_1\ 0_u^+$ molecular state. It can be shown [51,62] that the excited 0_u^+ $J = 1$ state is a mixture of $l = 0,2$ (s- and d-wave) partial waves, but not $l = 1$. Since in dipole transitions the rotational quantum number l must be conserved, the second photon can only transfer the excited molecule to $J = 0,2$ ground 0_g^+ states.

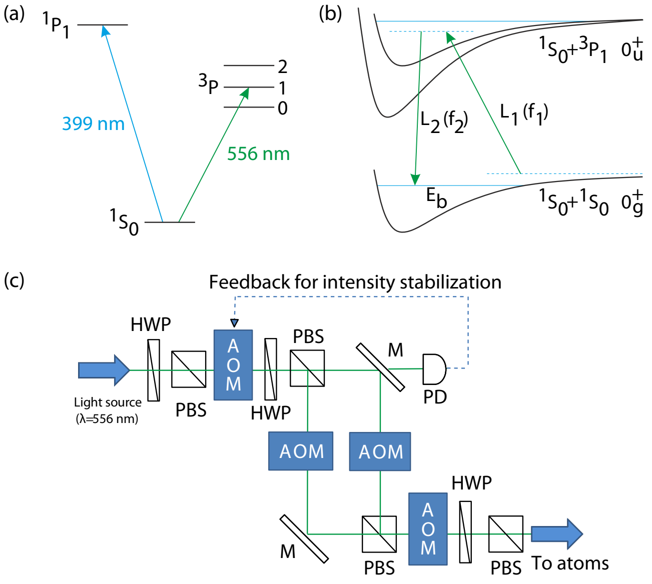

FIG. 1. (a) Main Yb transitions used in the experiment. (b) Two-color PA spectroscopy in a Raman configuration: a pair of 556 nm lasers transfer a colliding ground-state atomic pair to a ground molecular bound state through a virtual excited state. The difference between the laser frequencies $f_1 - f_2$ yields the bound-state energy E_b. (c) Schematic setup for PA lasers. The two laser beams for the Raman transition were split by a polarized beam splitter (PBS). The frequency difference between the two beams was controlled by acousto-optic modulators (AOMs). Two beams are combined by a PBS and then the polarization of both lights is set to be parallel to each other. In order to remove PA light-intensity fluctuations after optical fibers, we utilized an intensity-feedback system by use of an AOM and photodiode (PD). HWP: half-wave plate; M: mirror.

The schematic setup for the PA lasers is shown in Fig. 1(c). The two laser beams were prepared by splitting one laser beam of frequency-doubled light from a fiber laser operating at 1112 nm, coupled to the same optical fiber and delivered to Yb atoms. The slow drift of the laser frequency was suppressed by locking to an ultralow expansion cavity. The laser linewidth was about 100 kHz. The frequency difference between the two beams of L_1 and L_2 was controlled by acousto-optic modulators (AOMs). The radio-frequency sources of AOMs are generated by synthesizers 8648A (Agilent), which are stabilized with a 10 MHz clock from the GPS-stabilized synthesizer (DGPS-1.6, DS Technology, Japan). In order to remove PA light-intensity fluctuations after the optical fibers, we utilized an intensity-feedback system by use of an AOM and a photodiode (PD). Finally, the PA laser beams were aligned to pass through the atoms in the FORT by using a charge-coupled device camera for absorption imaging. The detuning of the PA laser with respect to the atomic resonance $^1S_0$-$^3P_1$ was easily checked by observing the frequency at which the atoms in the magneto-optical trap disappeared. The frequency f_1 of L_1 was fixed at a certain detuning from a $^1S_0 + {}^3P_1$ 0_u^+ PA resonance, and the frequency f_2 of L_2 was scanned to obtain spectra of the bound states in the Yb$_2$ ground state.

III. DETERMINATION OF BOUND-STATE ENERGIES

Each PA spectrum has been fitted with a Lorentzian line shape, and the observed linewidth was typically around several kHz. Peak positions suffered from systematic errors of three main origins: a light shift by two 556 nm PA lasers, a light shift by the 532 nm FORT light used to hold the atoms, and the mean-field shift of the BEC. Table I shows all of the measured binding energies in which the density shift and the light shifts from both the FORT and PA lasers are removed.

The light shift induced by the PA lasers is $\Delta E_{\mathrm{PA}}(I_{\mathrm{FB}}, I_{\mathrm{BB}}) = \alpha_{\mathrm{FB}} I_{\mathrm{FB}} + \alpha_{\mathrm{BB}} I_{\mathrm{BB}}$, where α_{FB} and α_{BB} are constants related to the Franck-Condon factors for the free-bound and bound-bound transitions, respectively, and similarly I_{FB} and I_{BB} are the laser intensities for free-bound and bound-bound transitions. In order to compensate the light shift by extrapolation, we measured the peak positions with several laser intensities for I_{FB} and I_{BB} and with ratio of $I_{\mathrm{FB}}/I_{\mathrm{BB}}$ kept constant. Figure 2(b) shows the light shift with several intensities for I_{BB} $(= I_{\mathrm{FB}})$. We removed the light shifts by extrapolation at $I_{\mathrm{FB}} = I_{\mathrm{BB}} = 0$. Typical shifts by PA light were of the order of less than 10 kHz.

The light shift by FORT light can be similarly eliminated, but one should be careful of the fact that changing the FORT

TABLE I. Measured and calculated binding energies E_b, in MHz, for bosonic homonuclear Yb$_2$ isotopologues. Vibrational quantum numbers v are numbered from the dissociation limit. J is the rotational quantum number. The reported binding energies can be compared to previous measurements in cold thermal gases [32] and to our theoretical models based on the same *ab initio* potential curve (Fig. 3): one purely Born-Oppenheimer ("reference") model and one that takes into account two beyond-Born-Oppenheimer (BBO) corrections—the adiabatic (DBOC) correction (Fig. 4) and the R dependence of the effective reduced mass μ (Fig. 5). The respective differences (in kHz) between the two theoretical models and the experimental data are also shown: it is interesting to notice that the reference model systematically yields binding energies lower than experimental for the two light isotopes (^{168}Yb and ^{170}Yb) and higher for the heavy ^{174}Yb isotope, whereas the BBO model does not—indicating significantly improved mass-scaling behavior. The average difference between the reference model and experiment is 112.9 kHz (rms), whereas for the BBO model this is reduced by almost a factor of four down to 30.2 kHz. For the purposes of future experiments, we provide extrapolated bound-state energies for two vibrational states below those investigated in our experiment. The last column gives the outer turning points R_t for the listed energy levels.

Molecule	v	J	Expt. (this work) (MHz)	Expt. [32] (MHz)	Reference model (MHz)	Diff. (kHz)	BBO model (MHz)	Diff. (kHz)	R_t/a_0
^{168}Yb$_2$	1	0			−0.79292		−0.79314		158.9
^{168}Yb$_2$	2	2	−145.53196(48)		−145.55804	−26.08	−145.53855	−6.59	66.6
^{168}Yb$_2$	2	0	−195.18141(46)		−195.27383	−92.41	−195.18711	−5.70	63.4
^{168}Yb$_2$	3	2			−1075.28866		−1075.03235		47.8
^{168}Yb$_2$	3	0			−1165.47490		−1165.08405		47.1
^{168}Yb$_2$	4	2			−3415.69550		−3415.03045		39.4
^{168}Yb$_2$	4	0			−3545.28999		−3544.42500		39.1
^{168}Yb$_2$	5	2			−7808.96845		−7807.68328		34.3
^{168}Yb$_2$	5	0			−7977.33871		−7975.79033		34.2
^{170}Yb$_2$	1	2	−3.66831(32)	−3.651(26)	−3.64732	+20.99	−3.66917	−0.86	123.1
^{170}Yb$_2$	1	0	−27.70024(44)	−27.661(23)	−27.69157	+8.67	−27.69224	+8.00	87.9
^{170}Yb$_2$	2	2	−398.05626(46)		−398.08462	−28.36	−398.06980	−13.54	56.4
^{170}Yb$_2$	2	0	−463.72552(80)		−463.83230	−106.78	−463.72705	−1.53	54.9
^{170}Yb$_2$	3	2	−1817.14074(80)		−1817.31174	−171.00	−1817.11393	+26.81	43.8
^{170}Yb$_2$	3	0	−1922.01467(505)		−1922.28419	−269.52	−1921.92989	+84.76	43.3
^{170}Yb$_2$	4	2			−4886.37405		−4885.90046		37.1
^{170}Yb$_2$	4	0			−5029.78536		−5029.09120		36.9
^{170}Yb$_2$	5	2			−10238.69119		−10237.71118		32.8
^{170}Yb$_2$	5	0			−10419.98838		−10418.72563		32.7
^{174}Yb$_2$	1	0	−10.62513(53)	−10.612(38)	−10.61266	+12.47	−10.62784	−2.71	103.1
^{174}Yb$_2$	2	2	−268.63656(56)	−268.75(21)	−268.49571	+140.85	−268.60620	+30.36	60.2
^{174}Yb$_2$	2	0	−325.66378(98)	−325.607(18)	−325.58245	+81.33	−325.62351	+40.27	58.3
^{174}Yb$_2$	3	2	−1432.82653(75)		−1432.70510	+121.44	−1432.85962	−33.09	45.5
^{174}Yb$_2$	3	0	−1527.88543(34)		−1527.86437	+21.06	−1527.88567	−0.24	45.0
^{174}Yb$_2$	4	2			−4088.59536		−4088.79949		38.2
^{174}Yb$_2$	4	0			−4220.99530		−4221.00440		38.0
^{174}Yb$_2$	5	2			−8846.73553		−8846.91201		33.6
^{174}Yb$_2$	5	0			−9015.82296		−9015.74456		33.5

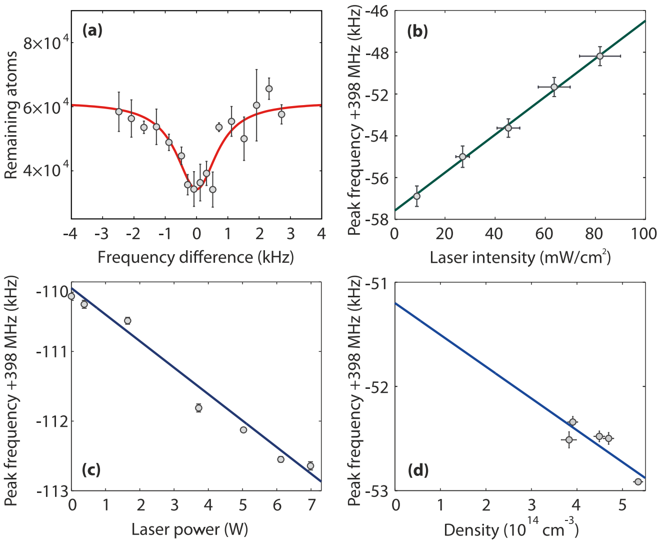

FIG. 2. Extrapolation of photoassociation line positions shown on the example of the ^{170}Yb $v = 2$, $J = 2$ line. (a) An example two-color PA spectrum fitted with a Lorentz function; the FWHM is about 1 kHz. (b) The optical light shift by the PA lasers as a function of laser intensity. (c) FORT light shift as measured by an additionally applied 532 nm laser as a function of its power. (d) Mean-field shift by the BEC as a function of atomic density. See Sec. III for details. The final Yb$_2$ binding energies are shown in Table I.

intensity not only changes the shift by FORT light, but also changes the atom density and, consequently, the mean-field energy. Therefore, instead of directly manipulating the FORT laser intensity, we measured light shifts to the atoms in an optical lattice due to another loosely focused light beam at the same wavelength, as shown in Fig. 2(c). The wavelength λ_L for the optical lattice is 532 nm and the potential depth is 15 E_R, where $E_R = h^2/(2m\lambda_L^2)$, where h is the Planck constant and m is the mass of the Yb atom. With this information, we estimated the light shift due to the FORT light by estimating the FORT intensity from measured trap parameters, such as the trap frequencies and FORT powers. Typical shifts by 532 nm light were of the order of a few kHz.

The remaining shift is the mean-field shift of the BEC. The mean-field energy is proportional to atomic density, and therefore the shift was removed similarly by extrapolation. Typical mean-field shifts were of the order of a few kHz, as shown in Fig. 2(d).

IV. THE INTERACTION MODELS

In this work, we will compare two approaches to the modeling of interactions in the Yb$_2$ molecule. First, we will construct a pure Born-Oppenheimer interaction model, following the standard procedure employed in previous mass-scaling analyses [14,28,32,51]. This will serve as a reference for comparison with a final model that incorporates additional beyond-Born-Oppenheimer (BBO) corrections.

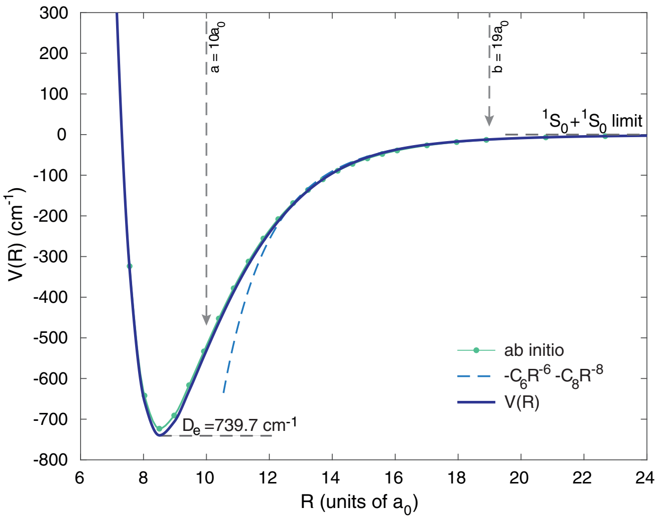

FIG. 3. The mass-independent Born-Oppenheimer potential curve $V(R)$ used to describe the ground 0_g^+ [or $^1\Sigma_g^+$ in Hund's case (a) notation] state of Yb$_2$. The short-range *ab initio* potential [58] (green dots) is interpolated using cubic splines, scaled by a fitted parameter s, and smoothly connected to an analytic $-C^6/R^6 - C^8/R^8$ long-range potential (dashed line) using a transition function described by Eq. (2) over the distances between $a = 10\,a_0$ and $b = 19\,a_0$. The depth of the fitted potential $D_e = 739.7$ cm^{-1}.

Within the Born-Oppenheimer approximation, the interactions between two ground-state $^1S_0$ atoms can be described by a single 0_g^+ ($^1\Sigma_g^+$) potential curve. The energy levels E_b for a given rotational quantum number J can be calculated using the radial Schrödinger equation of the form

$$\left[-\frac{\hbar^2}{2\mu}\frac{d^2}{dR^2} + V(R) + V'(R) + \frac{\hbar^2 J(J+1)}{2\mu R^2}\right]\Psi(R) = E_b\Psi(R). \tag{1}$$

The four Hamiltonian terms on the left-hand side are the radial kinetic energy, the mass-independent Born-Oppenheimer potential $V(R)$, the mass-dependent corrections $V'(R)$, and the rotational kinetic energy dependent on the rotational quantum number J. The reduced mass is denoted by μ. We calculate the bound-state solutions to this equation using the matrix discrete variable representation (DVR) technique [63] with a variation on the nonlinear coordinate transformation [64]. For the calculation of s-wave scattering lengths, we employ the renormalized Numerov method [65,66].

Our isotope-independent Born-Oppenheimer potential $V(R)$, shown in Fig. 3, consists of smoothly connected short- and long-range parts. The short-range part of the potential, $V_{\rm short}(R)$, is provided by cubic spline interpolation of the *ab initio* curve given in Ref. [58]. The long-range van der Waals part of the potential is analytic: $V_{\rm long}(R) = -C_6R^{-6} - C_8R^{-8}$. The short- and long-range parts are joined together using a transition function [67],

$$f(R) = \begin{cases} 0, & R \leqslant a \\ \frac{1}{2} + \frac{1}{4}\sin(\pi x/2)[3 - \sin^2(\pi x/2)], & a < R < b \\ 1, & b \leqslant R, \end{cases} \tag{2}$$

with $x = [(R-a)+(R-b)]/(b-a)$. The parameters $a = 10a_0$ and $b = 19a_0$ denote the transition region between the short- and long-range parts of the potential. The potential itself is calculated via $V(R) = [1 - f(R)]sV_{\rm short}(R) + f(R)V_{\rm long}$. For internuclear ranges $R < a$, the potential is purely *ab initio*, while for $R > b$, it is equal to $V_{\rm long}(R)$. Finally, s scales the *ab initio* potential, which, by modifying the potential depth D_e, enables us to fix the WKB phase ϕ to achieve mass scaling. This potential alone will be the basis of our reference Born-Oppenheimer potential, which will be compared to models incorporating beyond-Born-Oppenheimer (BBO) phenomena described below.

The isotopologue-dependent potential $V'(R)$ describes R-dependent molecular isotope shifts. Isotopic shifts of atomic energy levels are widely known phenomena in atomic spectroscopy which manifest themselves as static shifts to transition energies for different isotopes. During a collision, as atoms get closer together to form a molecule, the shape of their respective electronic clouds is modified. As a result, the isotopic shifts depend on the interatomic distance R. This gives rise to an additional, isotopologue-dependent, molecular potential $V'(R)$. As in atomic spectroscopy, the isotopic shift has two components: a mass shift and a volume shift. The former results from correlations between nuclear and electronic motion; the latter is due to the finite dimensions of the nuclei.

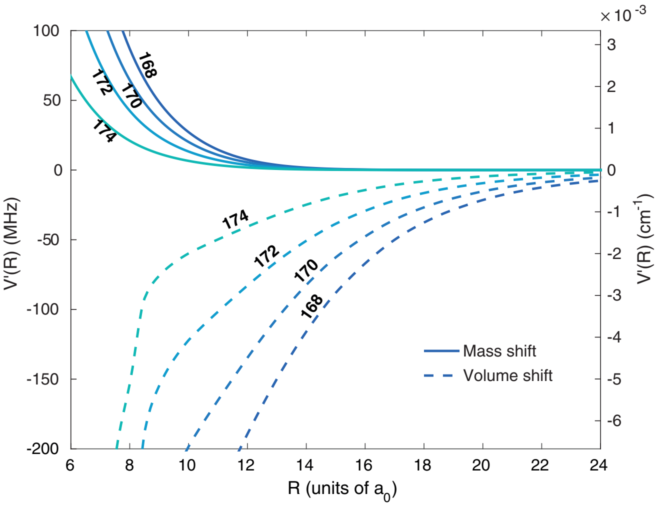

FIG. 4. Mass (solid lines) and volume (dashed lines) corrections to the interaction potential $V'(R)$ for bosonic isotopologues ^{168}Yb$_2$–^{174}Yb$_2$ with respect to ^{176}Yb$_2$, where they are defined as uniformly zero. The short-range parts of the curves are based on raw data published by the authors of Ref. [44] and, like the main potential $V(R)$, are smoothly connected to an analytic $A_6R^{-6} + A_8R^{-8}$ asymptote using Eq. (2). The mass shift depends on the nuclear reduced mass μ_n [Eq. (3)], while the volume shift is defined by the dimensions of the appropriate nuclei [Eq. (4)].

The essence of the Born-Oppenheimer approximation is that the electronic motion immediately follows that of the nuclei. In reality, however, the electrons also influence the nuclear motion through conservation of momentum. In atoms, this leads to the mass part of the isotopic shift. In molecules, this effect may be taken into account through the (perturbative) adiabatic or diagonal Born-Oppenheimer correction (DBOC) [42],

$$V'_{\rm mass}(R) = \sum_{i=1,2} \langle \Psi(\vec{r};\vec{R}_n)|\hat{T}_i|\Psi(\vec{r};\vec{R}_n)\rangle, \tag{3}$$

where $\hat{T}_i = -(\hbar^2/2m_{n,i})\hat{\nabla}_i^2$ are nuclear kinetic-energy operators for nuclear masses $m_{n,i}$, and the internuclear distance $R = |\vec{R}_1 - \vec{R}_2|$ depends on the positions of the two nuclei $\vec{R}_1$ and $\vec{R}_2$. The integration is carried over the electronic coordinates $\vec{r}$. Since in the BO approximation the electronic wave functions $\Psi_k(\vec{r};\vec{R}_n)$ are isotope independent, the adiabatic correction is proportional to $1/m_{n,1} + 1/m_{n,2} = 1/\mu_n$. The off-diagonal matrix elements of the same operator lead to nonadiabatic corrections. For Yb$_2$, the adiabatic corrections have been recently calculated with respect to the ^{176}Yb$_2$ isotopologue using modern quantum chemistry methods and raw data have been made available [44]. The asymptotic long-range behavior of the adiabatic correction is $A_6R^{-6} + A_8R^{-8} + \cdots$ [68] (for instance, in H$_2$, $A_6 = (5/\mu)\,C_6$ [69]). Much like our potential, the *ab initio* points are interpolated and smoothly connected by Eq. (2) with an analytic $A_6^{\rm mass}R^{-6} + A_8^{\rm mass}R^{-8}$ long range. In this case, however, the long-range coefficients $A_6^{\rm mass}$ and $A_8^{\rm mass}$ were fitted to the *ab initio* points. The adiabatic correction curve is appropriately mass scaled to the isotopologue at hand. The resulting curves are shown in Fig. 4. Note that these curves are given with respect to the ^{176}Yb$_2$ isotopologue. As a consequence, the potential coefficients given in Table II also reflect the (heaviest) ^{176}Yb$_2$ case. The largest adiabatic corrections to C_6 are for the lightest isotopologue, ^{168}Yb, and are equal to $A_6^{\rm mass} = -0.00202$ and $A_8^{\rm mass} = 0.750541$ atomic units.

The nuclear volume effect stems from the finite, and isotope-dependent, dimensions of the nuclei. Outside the nucleus, the electron-nuclei interactions have the typical Coulomb character. Inside the nucleus, however, the electric field has lower magnitude. This has the effect of making the electron-nuclei interaction energy slightly higher. In a first-order approximation, the magnitude of this effect depends on the nuclear rms charge radii $\langle r^2\rangle$ and the density of the

TABLE II. Long-range Yb$_2$ ground-state 0_g^+ potential parameters C_6, C_8 and potential depths D_e from different sources compared to our determinations: the reference Born-Oppenheimer model and one that takes into account two BBO effects—the adiabatic Born-Oppenheimer correction based on [44] and the distance dependence of the effective reduced mass μ. It is important to note that the C_6 and C_8 values are given for the ^{176}Yb$_2$ isotopologue—the adiabatic correction introduces a slight variation of these parameters from isotope to isotope.

	C_6 (10^3 a.u.)	C_8 (10^5 a.u.)	D_e (cm^{-1})	χ^2
Ab initio [58]	2.57		723.7	
Ab initio [75,76]	1.929(39)	1.88(6)		
Previous PA [32]	1.932(30)	1.9(5)		
Reference model	1.9335(22)	2.172(65)	743.0(2.4)	220792
BBO model	1.93727(57)	2.265(17)	739.73(60)	9555

electrons at the center of the nucleus [43]:

$$V'_{\text{volume}}(R) = \frac{2\pi}{3} Z\left(\frac{e^2}{4\pi\epsilon_0}\right)|\Psi(0)|^2\lambda_{A,A'}, \tag{4}$$

where $\lambda_{A,A'} = \langle r_{A'}^2\rangle - \langle r_A^2\rangle$ is the difference in rms nuclear radii between the isotope at hand and a reference isotope—in our case ^{176}Yb—and can be taken from the database [70]. The contact density $|\Psi(0)|^2$ for Yb$_2$ has also been calculated in Ref. [44]. In this case, however, the authors of Ref. [44] warn that the density functional theory (DFT)-based method used for their calculation was shown to be inadequate for the simpler system of Sr$_2$ and that their results should be considered qualitative estimates. Like the mass shift, we fit the contact densities with a $A_6^{\text{volume}}R^{-6} + A_8^{\text{volume}}R^{-8}$ long range [71] and interpolate using Eq. (2). The volume shift itself is then calculated from Eq. (4) bearing in mind that there are two nuclei in a diatomic molecule and contributions from both need to be taken into account. The resulting correction curves are shown in Fig. 4.

There are two fundamental interpretations of the Born-Oppenheimer picture [44]. One can be described as a "physicist's molecule"—a molecule is composed of two distinct atoms of mass $m_{a,1}$ and $m_{a,2}$ bound by an interaction potential $V(R)$. In this picture, the reduced mass in Eq. (1) should be calculated from the *atomic* masses, $\mu_a = (m_{a,1}^{-1} + m_{a,2}^{-1})^{-1}$. This picture is well grounded especially at large atomic separations, beyond the LeRoy radius R_{LR} [72] where each atoms' electrons move together with the nuclei. This is manifestly appropriate in photoassociation spectroscopy, where the probed molecules are very weakly bound, and in scattering calculations, where whole atoms are considered as colliding bodies. In particular, scattering lengths are defined for atomic masses. On the other hand, at small internuclear separations, a "chemist's molecule" picture is more relevant. Here, the nuclei move in accordance with an effective potential $V(R)$ created by the interplay between the nuclei and the electron cloud. In this case, we should put the *nuclear* mass $\mu_n = (m_{n,1}^{-1} + m_{n,2}^{-1})^{-1}$ into the radial Schrödinger equation.

The duality between the chemist's and physicist's pictures may be eliminated by consistent accounting for nonadiabatic corrections [45,46]. A more practical way to transition between two regimes by means of distance-dependent reduced masses has been tackled previously [47,49,50], although only for very small molecules [48,73]. Using effective reduced masses enables us to partially account for nonadiabatic effects. For large systems, such as Yb$_2$, no *ab initio* data are available; therefore we resort to an empirical approach where we model the reduced masses with an analytic function of the form

$$\mu(R) = \mu_a - \frac{\mu_a - \mu_n}{1 + (R_m/R)^6}, \tag{5}$$

shown in Fig. 5(a) for $R_m = 18a_0$. This function was chosen for the following reasons:

(i) at short ranges, as $R \to 0$, $\mu(R) \to \mu_n$;

(ii) at long ranges, as $R \to \infty$, $\mu(R) \to \mu_a$;

(iii) for large R, $\mu(R)$ approaches μ_a as R^{-6}, following Ref. [47].

The quantity R_m serves as a range parameter that defines the point where the $\mu(R)$ is exactly halfway between μ_a and μ_n. The atomic masses m_a were taken from Ref. [74]; the nuclear masses are, of course, 70 electron masses lower.

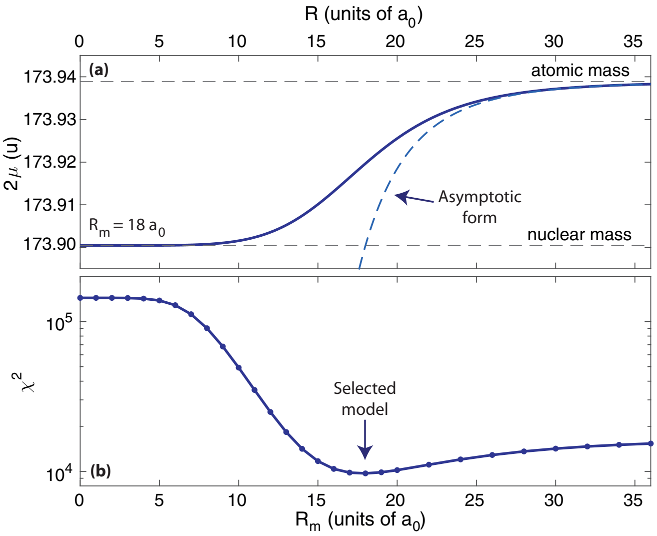

FIG. 5. (a) The effective, distance-dependent reduced mass as defined by Eq. (5) shown for the ^{174}Yb$_2$ isotopomer. The R_m parameter defines the distance where the effective mass $\mu(R)$ is exactly halfway between the nuclear μ_n and atomic μ_a reduced masses. At shorter distances, μ is closer to the nuclear mass limit, while as $R \to \infty$, μ approaches the atomic reduced mass as R^{-6}. The case of $R_m = 18\,a_0$ shown in the figure is used in our BBO model. (b) The dependence of fit quality factor χ^2 for the BBO interaction model as a function of the effective mass range parameter R_m. The lowest $\chi^2 = 9555$ (χ^2/dof = 1062) is reached for $R_m = 18\,a_0$.

In this analysis, we will assume the same $\mu(R)$ for the vibrational and rotational motion. In general, the two will differ: for example, Pachucki and Komasa [47], in their general nonadiabatic framework for a diatomic molecule, give different expressions for the vibrational $\mu_\parallel$ and rotational $\mu_\perp$ reduced masses. Also, these functions may not be as well behaved as Eq. (5). For example, the effective vibrational reduced mass $\mu_\parallel$ for H$_2$ of Ref. [48] actually exceeds μ_a before reaching the appropriate asymptotic value.

V. RESULTS

The first step in our analysis is the construction of the reference Born-Oppenheimer interaction model where no mass-dependent effects are taken into account. The potential parameters C_6, C_8, and D_e are fitted using the least-squares method, i.e., by minimizing the fit parameter $\chi^2 = \sum_{i=1}^{N}(E_i^{\text{th}} - E_i^{\text{expt}})^2/u_i^2$ using the Levenberg-Marquardt algorithm. The outer turning points of the vibrational states are well beyond the LeRoy radius R_{LR} [72] and the corresponding vibrational spacings depend mostly on the long-range C_6 coefficient [79]. On the other hand, the position of the entire near-dissociation vibrational series for a given isotope depends on the zero-energy WKB phase,

$$\phi = \frac{1}{\hbar}\int_{R_{\text{in}}}^{\infty}\sqrt{-2\mu V(R)}dR, \tag{6}$$

integrated from the potential's inner turning point R_{in} to infinity. Assuming a mass-independent potential and a fixed reduced mass μ, this phase is explicitly proportional to $\sqrt{\mu}$. In mass-scaling analyses of photoassociation data or scattering lengths, it is usually assumed that $\mu = \mu_a$. The number of vibrational bound states supported by a potential with a R^{-6} long range is $N = \lfloor \phi/\pi + 3/8 \rfloor$ [31]. In order for a potential to be mass scaled, i.e., correctly describe the energy level positions for all isotopes characterized by different reduced masses μ, the potential curve has to support the correct number of bound states.

In our case, mass scaling is reached when the ground state ^{174}Yb molecule has 72 vibrational states for rotational angular momentum $J = 0$ (the same as in a previous determination [51]). Any attempts to change the number of bound states result in a χ square that is many orders of magnitude larger. The parameters of the reference fit that uses only a Born-Oppenheimer curve are shown in Table II. The theoretical bound-state energies provided by this model are shown in Table I. This fit, and its χ^2 of 220 792 (and χ square per degree of freedom $\chi^2/\text{dof} = 24\,532$) will serve as a reference for further fits using additional mass-dependent effects. The type-B uncertainties in Table II are calculated using the mean rms differences between theoretical and experimental bound-state energies. For the reference model, these are equal to 112.9 kHz.

The first attempted improvement to the model was to add the isotopic mass shifts (Fig. 4) calculated in Ref. [44]. This resulted in a decrease of χ^2 by about 35%, down to 143 856 ($\chi^2/\text{dof} = 15\,984$), with very little impact on potential parameters. The situation changes when the mass effect is replaced by the nuclear volume effect. In this case, the fit falls apart—χ^2 becomes over 30 times larger than that of our reference fit and exceeds 8×10^6 ($\chi^2/\text{dof} = 892\,942$). Also, both van der Waals coefficients C_6 and C_8 change considerably; in this fit, $C_6 \approx 1.922 \times 10^3$ a.u., which is incompatible with the reference fit. Finally, a fit that includes both the mass and nuclear volume effects inherits the weaknesses caused by adding the nuclear volume effect and is characterized by a similarly high χ^2 of about 7.5×10^6 ($\chi^2/\text{dof} = 828529$). The explanation could be that the two corrections work in opposite directions. As isotope mass increases, the mass effect will tend to decrease the potential depth for lighter isotopes, while the significantly larger nuclear volume effect will make the effective potential deeper (see Fig. 4). This does not necessarily mean that the sign of this correction is wrong—it may simply be overestimated. The authors of Ref. [44] warn that their nuclear volume effect calculations are of lower quality than those of the mass effect. In the future, more accurate calculations may be feasible. For now, we continue with a model that takes only the mass effect (i.e., the adiabatic correction) into account.

By far, the best improvement is reached by including the distance-dependent effective mass. Our empirical model of the effective mass has a range parameter R_m which defines the transition point between the nuclear-mass and atomic-mass limits. We run a series of fits for a model that includes the adiabatic correction with different values of R_m, and show their respective χ^2 in Fig. 5(b). A minimum of $\chi^2 = 9555$ ($\chi^2/\text{dof} = 1062$) is found for $R_m = 18a_0$, which is an improvement by a factor of 23 with respect to the reference model. We have also verified that including the nuclear volume effect again results in a serious deterioration of the quality of the fit: for all tested values of R_m, the value of $\chi^2 > 4.8 \times 10^6$, whether with or without the DBOC correction. Finally, we note that an accidentally slightly better χ^2 of about 9175 is obtained if we take only the Born-Oppenheimer potential and the nuclear reduced mass μ_n (equivalent to $R_m \to \infty$). Such a model, however, would prevent us from calculating the s-wave scattering lengths for which it is necessary that the reduced mass for atoms separated as $R \to \infty$ be equal to m_a.

Dissociation energy D_e and long-range C_6, C_8 coefficients obtained with the final model, which incorporates the mass shift and the effective mass, are shown in the last row of Table II. A comparison of experimental and the theoretical bound-state energies produced using this model is given in Table I. The average differences between this model and the experimental data are 30.2 kHz (rms), which is an improvement by a factor of about 3.7 over the reference model.

Our value of $R_m = 18a_0$ nicely coincides with the LeRoy radius $R_{\text{LR}} = 2(\tilde{R}_A + \tilde{R}_B) = 16.78\,a_0$ (for Yb$_2$, the rms atomic radii $\tilde{R}_A = \tilde{R}_B = 2.22$ Å [80]). Mass scaling appears to be governed mostly by the nuclear mass μ_n as most of the WKB phase of a bound-state wave function originates from the potential well ($R < R_{\text{LR}}$). On the other hand, the vibrational spacings are governed mostly by the long-range part of the potential ($R > R_{\text{LR}}$), where the atoms are well separated and the van der Waals $-C_6R^{-6} - C_8R^{-8}$ interaction dominates. Since R_{LR} is a much shorter distance than the outer turning points of bound states probed in our experiment, their vibrational spacings alone would be governed by the atomic mass μ_a. This explains why interaction models based on atomic masses were thus far successful in the description of photoassociation spectra.

By looking at the differences between theoretical and experimental bound-state energies (Table I), we can verify that the gain in the quality of the fit is at least partially due to the improved representation of the mass-scaling behavior. The reference model tends to give bound-state energies that are too low in the two light isotopes (i.e., most differences have a negative sign) and energies too high for ^{176}Yb, while the differences for the BBO model seem a lot more random. In fact, the average differences for the reference model are +83(35) kHz for ^{168}Yb and ^{170}Yb together, and −75(26) kHz for ^{174}Yb clearly showing signs of a mass-dependent systematic shift. For the BBO model, the average differences are −11(12) kHz for the two light isotopes and −7(11) kHz for ^{176}Yb. Both are statistically compatible with zero and no longer provide grounds to suspect a mass-dependent systematic shift. Similarly, the Pearson correlation coefficient between atomic masses and the residuals for the reference model is $\rho_{\text{Ref}} = 0.636$ and is statistically significant at a p value of $p = 0.019$, while for the BBO model, it is not: $\rho_{\text{BBO}} = 0.009$ at $p = 0.987$.

No experimental data for the deep parts of the Yb$_2$ potential curve are available at this point. There is therefore currently no way to compare our $D_e = 739.73(60)\,\text{cm}^{-1}$ to experiment. The only way photoassociation data is sensitive to the short-range potential is through mass scaling, which in our case dictates the number of bound states supported by the potential curve—

72 for ^{174}Yb. On the other hand, the model potentials in the previous analyses [32,51] also supported 72 states, but their depth in itself was closer to 1000 cm^{-1}. This difference is due to a differently located inner turning point and the different shape of the potential well. Still, our fitted potential depth $D_e = 739.73(60)$ cm^{-1} is only about 2.2% deeper than the original *ab initio* curve with $D_e = 723.7$ cm^{-1}.

On the other hand, our van der Waals coefficients can be compared to previous *ab initio* and spectroscopic determinations, as shown in Table II. Our $C_6 = 1.93727(57) \times 10^3$ a.u. coefficient agrees both with the empirical determination of $C_6 = 1.932(30) \times 10^3$ a.u. based on a previous thermal PA experiment [32] and the *ab initio* determination of $C_6 = 1.929(39) \times 10^3$ of Safronova *et al.* [75]. The $C_6 = 1.9335(22) \times 10^3$ value of the reference model is also in agreement (though less precise) with the BBO model. On the other hand, our C_8 coefficient is about 20% larger than both the previous PA [32,51] and *ab initio* [76] determinations. This difference could stem from the fact that C_8 operates at shorter internuclear distances than C_6 and may be—from the point of view of bound-state energies—partially obfuscated by the actual shape of the potential: C_n terms beyond C_8 that naturally exist in a potential may contribute to an "effective" C_8.

Finally, we use our interaction models to calculate the s-wave scattering lengths for all bosonic pairs of Yb isotopes. The s-wave scattering length is a shift to the atomic collisional wave function due to the atomic interaction, in the limit of zero kinetic energy. At large nuclear separations R, the wave function for an s-wave collision is asymptotically $\Psi(R) \sim \sin[k(R-a)]$, where a is the scattering length, and k is the wave number for a given collisional energy ϵ. At large distances, the atoms are well separated, and the quantum wave number is calculated using the atomic, rather than nuclear, reduced mass μ_a: $k = \sqrt{2\mu_{\mathrm{at}}\epsilon}/\hbar$. The scattering length is calculated by taking the limit of zero kinetic energy or, equivalently, $k \to 0$. Like in the case of the potential parameters, the uncertainties are based on the quality of the fit and were propagated from the parameter covariance matrix via $\tilde{u}^2(a) = \sum_{i,j}(\partial a/\partial p_i)(\partial a/\partial p_j)\,\mathrm{Cov}_{i,j}$.

The scattering lengths and their respective uncertainties calculated from both interaction models are given in Table III. Their values, regardless of the model, are in agreement with previous photoassociation-based determination of Kitagawa *et al.* [32], but the uncertainties are improved by over two orders of magnitude. The scattering lengths calculated from both models are mostly in agreement with each other to within 1–2 mutual uncertainties. The error bars for the BBO model, however, are a factor of 4 more stringent than those from the mass-independent reference model. Our scattering lengths may also be compared to those determined (or at least confirmed previously) using other methods. BEC expansion-based measurements of ^{170}Yb [60] and ^{174}Yb [59] scattering lengths gave the values of $+3.6(0.9)$ nm and $+6^{+10}_{-5}$ nm, respectively, corresponding to stable condensates with repulsive interactions. The results of the expansion of ^{168}Yb condensates were found to be consistent with the previously reported PA-based [32] value of $+13.33(18)$ nm. Similarly, the unstable behavior of ^{176}Yb for large atom numbers, on the other hand, was found to be well explained by its small negative scattering length. The apparent lack of interactions between ^{168}Yb and ^{174}Yb BEC clouds reported in Ref. [61] points at a near-zero interspecies scattering length. Finally, the large negative scattering lengths effectively thwart any attempts to produce a ^{172}Yb BEC or a ^{170}Yb-^{174}Yb BEC mixture.

TABLE III. Yb s-wave scattering lengths for collisions of bosonic isotopes calculated using best-fit Born-Oppenheimer ("Reference model") and beyond-Born-Oppenheimer ("BBO model") interaction models. Previously reported values derived from the expansion of ^{168}Yb [61], ^{170}Yb [60], and ^{174}Yb [59] BECs, one-color photoassociation spectroscopy [77], as well as stability of attractive BECs [78] and BEC mixtures [61] are shown in the column "Previous determinations." Calculations of s-wave scattering lengths based on two-color photoassociation spectroscopy of ultracold thermal Yb gases ("PA [32]") are also given for comparison and are in perfect agreement with the present determination. The error bars of the BBO model are about four times smaller, reflecting the improved quality of the fit thanks to the additional physics taken into account (see Sec. IV for details). The scattering lengths derived from the two models agree for the most part to within 1–2 mutual uncertainties. All values are given in nm.

Isotope 1	Isotope 2	Previous determinations	Comment	2PA [32]	Reference model	BBO model
168	168	Consistent with +13.33(18) [61]	BEC expansion	+13.33(18)	+13.380(11)	+13.3807(32)
170	170	+3.6(0.9) [60]	BEC expansion	+3.38(11)	+3.3845(14)	+3.38443(46)
172	172	(large, negative)	No stable BEC formation	−31.7(3.4)	−31.12(14)	−31.366(46)
174	174	+5.53(11) [77] +6(+10,−5) [59]	One-color photoassociation BEC expansion	+5.55(8)	+5.5601(16)	+5.55812(50)
176	176	Consistent with −1.28(23) [78]	Instability of large BECs	−1.28(23)	−1.2596(51)	−1.2749(17)
168	170			+6.19(8)	+6.2044(18)	+6.20565(56)
168	172			+3.44(10)	+3.4459(16)	+3.44583(45)
168	174	(small) [61]	Stability of binary BEC	+0.13(18)	+0.1412(32)	+0.1371(11)
168	176			−19.0(1.6)	−18.803(60)	−18.907(20)
170	172			−0.11(19)	−0.0973(35)	−0.1019(12)
170	174	(large, negative)	No stable binary BEC	−27.4(2.7)	−26.96(11)	−27.151(36)
170	176			+11.08(12)	+11.1047(65)	+11.0955(20)
172	174			+10.61(12)	+10.6346(60)	+10.6264(18)
172	176			+5.62(8)	+5.6275(15)	+5.62548(50)
174	176			+2.88(12)	+2.8912(17)	+2.88760(50)

VI. CONCLUSION

A total of 13 energy levels for three isotopologues of the ground-state Yb_2 dimer were probed by two-color photoassociation spectroscopy in a gas of ytterbium atoms. By performing the PA spectroscopy in a narrow line Raman scheme in a Bose-Einstein condensate and through a careful examination of systematic shifts, the accuracy of the measurement reaches $\approx$500 Hz. The experimental data was analyzed using *ab initio* based, mass-scaled Born-Oppenheimer interaction models. We show that by including beyond-Born-Oppenheimer effects (the adiabatic corrections and a distance-dependent reduced mass), we are able to improve the fit of the theoretical model from about 112.9 to 30.2 kHz on average (rms). We give improved van der Waals coefficients and determine the s-wave scattering lengths with error bars at the picometer level—over two orders of magnitude better than previous determinations.

Photoassociation spectroscopy is now extremely accurate and the construction of theoretical models for the data it produces is an increasingly challenging task. Beyond-Born-Oppenheimer corrections, especially distance-dependent effective masses, will be critical for future attempts at reaching kHz accuracies in mass-scaled models. For heavy systems, only qualitative calculations of isotopic shifts have recently appeared [44]. In our work, we show that while the inclusion of the mass effect (i.e., the adiabatic Born-Oppenheimer correction) leads to better theoretical description of the experimental data, the volume effect, however, was found to have a detrimental effect on the quality of the fit. Further *ab initio* calculations of the volume shifts will be necessary to verify the accuracy of their initial estimation. Nonadiabatic effects, partially treated here through effective masses, also have an impact on the atomic interactions and it may turn out that the effective nonadiabatic potential [47] cancels out at least partially with the volume effect. At this point, no *ab initio* calculations of the effective nonadiabatic potentials for heavy systems are available, although a very recent full treatment of nonadiabatic effects [73], including R-dependent masses, for He_2 raises hope for similar works for other molecules composed of divalent atoms. Mass-scaled interaction models, apart from their utility for precise calculation of scattering properties, are also proposed as a means to provide experimental constraints on Yukawa-type fifth forces [81]. Such attempts, however, will require the theory to match experimental data to well below 1 kHz.

ACKNOWLEDGMENTS

We acknowledge K. Enomoto, M. Ando, J. Hutson, E. Tiemann, and R. Moszyński for their useful comments. This work has been partially supported by the Grant-in-Aid for Scientific Research of JSPS (Grants No. JP25220711, No. JP26247064, No. 16H00990, No. 16H01053, and No. JP17H06138), Impulsing Paradigm Changing Through Disruptive Technologies (ImPACT) program, and JST CREST (Grant No. JPMJCR1673). We acknowledge partial support by Russian Science Foundation Grant No. 17-13-01466. This research was partially supported by the TEAM Programme of the Foundation for Polish Science (Project No. TEAM/2010-6/3), co-financed by the EU European Regional Development Fund. This research was also partially supported by the COST Action CM1405 MOLIM. We acknowledge support from the National Science Centre (Grant No. 2014/13/N/ST2/02591). It has also received funding from the EMPIR programme co-financed by the Participating States and from the European Union Horizon 2020 research and innovation programme (EMPIR 15SIB03 OC18). It is part of an ongoing research program of the National Laboratory FAMO in Toruń, Poland. Calculations have been carried out at the Wroclaw Centre for Networking and Supercomputing (http://www.wcss.pl), Grant No. 353.

---

[1] K. M. Jones, E. Tiesinga, P. D. Lett, and P. S. Julienne, Rev. Mod. Phys. **78**, 483 (2006).
[2] J. L. Bohn and P. S. Julienne, Phys. Rev. A **60**, 414 (1999).
[3] H. R. Thorsheim, J. Weiner, and P. S. Julienne, Phys. Rev. Lett. **58**, 2420 (1987).
[4] V. Bagnato, L. Marcassa, C. Tsao, Y. Wang, and J. Weiner, Phys. Rev. Lett. **70**, 3225 (1993).
[5] P. D. Lett, K. Helmerson, W. D. Phillips, L. P. Ratliff, S. L. Rolston, and M. E. Wagshul, Phys. Rev. Lett. **71**, 2200 (1993).
[6] L. P. Ratliff, M. E. Wagshul, P. D. Lett, S. L. Rolston, and W. D. Phillips, J. Chem. Phys. **101**, 2638 (1994).
[7] J. D. Miller, R. A. Cline, and D. J. Heinzen, Phys. Rev. Lett. **71**, 2204 (1993).
[8] R. A. Cline, J. D. Miller, and D. J. Heinzen, Phys. Rev. Lett. **73**, 632 (1994).
[9] G. Zinner, T. Binnewies, F. Riehle, and E. Tiemann, Phys. Rev. Lett. **85**, 2292 (2000).
[10] C. Degenhardt, T. Binnewies, G. Wilpers, U. Sterr, F. Riehle, C. Lisdat, and E. Tiemann, Phys. Rev. A **67**, 043408 (2003).
[11] S. B. Nagel, P. G. Mickelson, A. D. Saenz, Y. N. Martinez, Y. C. Chen, T. C. Killian, P. Pellegrini, and R. Cote, Phys. Rev. Lett. **94**, 083004 (2005).
[12] T. Zelevinsky, M. M. Boyd, A. D. Ludlow, T. Ido, J. Ye, R. Ciuryło, P. Naidon, and P. S. Julienne, Phys. Rev. Lett. **96**, 203201 (2006).
[13] S. Stellmer, B. Pasquiou, R. Grimm, and F. Schreck, Phys. Rev. Lett. **109**, 115302 (2012).
[14] M. Borkowski, P. Morzyński, R. Ciuryło, P. S. Julienne, M. Yan, B. J. DeSalvo, and T. C. Killian, Phys. Rev. A **90**, 032713 (2014).
[15] Y. Takasu, K. Komori, K. Honda, M. Kumakura, T. Yabuzaki, and Y. Takahashi, Phys. Rev. Lett. **93**, 123202 (2004).
[16] S. Tojo, M. Kitagawa, K. Enomoto, Y. Kato, Y. Takasu, M. Kumakura, and Y. Takahashi, Phys. Rev. Lett. **96**, 153201 (2006).
[17] U. Marvet and M. Dantus, Chem. Phys. Lett. **245**, 393 (1995).
[18] R. Ciuryło, E. Tiesinga, S. Kotochigova, and P. S. Julienne, Phys. Rev. A **70**, 062710 (2004).
[19] R. Wynar, R. S. Freeland, D. J. Han, C. Ryu, and D. J. Heinzen, Science **287**, 1016 (2000).
[20] U. Schlöder, T. Deuschle, C. Silber, and C. Zimmermann, Phys. Rev. A **68**, 051403(R) (2003).
[21] R. Dumke, J. D. Weinstein, M. Johanning, K. M. Jones, and P. D. Lett, Phys. Rev. A **72**, 041801 (2005).

[22] J. L. Bohn and P. S. Julienne, Phys. Rev. A **54**, R4637 (1996).

[23] E. R. I. Abraham, W. I. McAlexander, C. A. Sackett, and R. G. Hulet, Phys. Rev. Lett. **74**, 1315 (1995).

[24] C. C. Tsai, R. S. Freeland, J. M. Vogels, H. M. J. M. Boesten, B. J. Verhaar, and D. J. Heinzen, Phys. Rev. Lett. **79**, 1245 (1997).

[25] C. Lisdat, N. Vanhaecke, D. Comparat, and P. Pillet, Eur. Phys. J. D **21**, 299 (2002).

[26] K. Winkler, G. Thalhammer, M. Theis, H. Ritsch, R. Grimm, and J. H. Denschlag, Phys. Rev. Lett. **95**, 063202 (2005).

[27] F. Münchow, C. Bruni, M. Madalinski, and A. Görlitz, Phys. Chem. Chem. Phys. **13**, 18734 (2011).

[28] M. Borkowski, P. S. Żuchowski, R. Ciuryło, P. S. Julienne, D. Kędziera, Ł. Mentel, P. Tecmer, F. Münchow, C. Bruni, and A. Görlitz, Phys. Rev. A **88**, 052708 (2013).

[29] S. Dutta, J. Pérez-Ríos, D. S. Elliott, and Y. P. Chen, Phys. Rev. A **95**, 013405 (2017).

[30] F. Dalfovo, S. Giorgini, L. P. Pitaevskii, and S. Stringari, Rev. Mod. Phys. **71**, 463 (1999).

[31] G. F. Gribakin and V. V. Flambaum, Phys. Rev. A **48**, 546 (1993).

[32] M. Kitagawa, K. Enomoto, K. Kasa, Y. Takahashi, R. Ciuryło, P. Naidon, and P. S. Julienne, Phys. Rev. A **77**, 012719 (2008).

[33] E. Pachomow, V. P. Dahlke, E. Tiemann, F. Riehle, and U. Sterr, Phys. Rev. A **95**, 043422 (2017).

[34] Y. N. M. de Escobar, P. G. Mickelson, P. Pellegrini, S. B. Nagel, A. Traverso, M. Yan, R. Côté, and T. C. Killian, Phys. Rev. A **78**, 062708 (2008).

[35] Y. B. Band and A. Vardi, Phys. Rev. A **74**, 033807 (2006).

[36] Z. Yu and C. J. Pethick, Phys. Rev. Lett. **104**, 010801 (2010).

[37] Y. B. Band and I. Osherov, Phys. Rev. A **84**, 013822 (2011).

[38] A. D. Ludlow, M. M. Boyd, J. Ye, E. Peik, and P. O. Schmidt, Rev. Mod. Phys. **87**, 637 (2015).

[39] L. Franchi, New J. Phys. **19**, 103037 (2017).

[40] R. Bouganne, M. B. Aguilera, A. Dareau, E. Soave, J. Beugnon, and F. Gerbier, New J. Phys. **19**, 113006 (2017).

[41] B. J. Verhaar, E. G. M. van Kempen, and S. J. J. M. F. Kokkelmans, Phys. Rev. A **79**, 032711 (2009).

[42] M. Born and K. Huang, *Dynamical Theory of Crystal Lattices* (Oxford University, New York, 1956).

[43] J. Schlembach and E. Tiemann, Chem. Phys. **68**, 21 (1982).

[44] J. J. Lutz and J. M. Hutson, J. Mol. Spectrosc. **330**, 43 (2016).

[45] W. Kolos and L. Wolniewicz, J. Chem. Phys. **41**, 3674 (1964).

[46] W. Kołos and L. Wolniewicz, J. Chem. Phys. **43**, 2429 (1965).

[47] K. Pachucki and J. Komasa, J. Chem. Phys. **129**, 034102 (2008).

[48] K. Pachucki and J. Komasa, J. Chem. Phys. **130**, 164113 (2009).

[49] P. Bunker and R. Moss, Mol. Phys. **33**, 417 (1977).

[50] W. Kutzelnigg, Mol. Phys. **105**, 2627 (2007).

[51] M. Borkowski, R. Ciuryło, P. S. Julienne, S. Tojo, K. Enomoto, and Y. Takahashi, Phys. Rev. A **80**, 012715 (2009).

[52] M.-S. Kim, J. Lee, J. H. Lee, Y. Shin, and J. Mun, Phys. Rev. A **94**, 042703 (2016).

[53] M. Borkowski, R. Ciuryło, P. S. Julienne, R. Yamazaki, H. Hara, K. Enomoto, S. Taie, S. Sugawa, Y. Takasu, and Y. Takahashi, Phys. Rev. A **84**, 030702 (2011).

[54] Y. Takasu, Y. Saito, Y. Takahashi, M. Borkowski, R. Ciuryło, and P. S. Julienne, Phys. Rev. Lett. **108**, 173002 (2012).

[55] P. O. Fedichev, Y. Kagan, G. V. Shlyapnikov, and J. T. M. Walraven, Phys. Rev. Lett. **77**, 2913 (1996).

[56] R. Ciuryło, E. Tiesinga, and P. S. Julienne, Phys. Rev. A **71**, 030701(R) (2005).

[57] K. Enomoto, K. Kasa, M. Kitagawa, and Y. Takahashi, Phys. Rev. Lett. **101**, 203201 (2008).

[58] A. A. Buchachenko, G. Chałasiński, and M. M. Szczęśniak, Eur. Phys. J. D **45**, 147 (2007).

[59] Y. Takasu, K. Maki, K. Komori, T. Takano, K. Honda, M. Kumakura, T. Yabuzaki, and Y. Takahashi, Phys. Rev. Lett. **91**, 040404 (2003).

[60] T. Fukuhara, S. Sugawa, and Y. Takahashi, Phys. Rev. A **76**, 051604(R) (2007).

[61] S. Sugawa, R. Yamazaki, S. Taie, and Y. Takahashi, Phys. Rev. A **84**, 011610(R) (2011).

[62] F. H. Mies, W. J. Stevens, and M. Krauss, J. Mol. Spectrosc. **72**, 303 (1978).

[63] D. T. Colbert, W. H. Miller, D. T. Colbert, and W. H. Miller, J. Chem. Phys. **96**, 1982 (1992).

[64] E. Tiesinga, C. J. Williams, and P. S. Julienne, Phys. Rev. A **57**, 4257 (1998).

[65] B. R. Johnson, J. Chem. Phys. **67**, 4086 (1977).

[66] B. R. Johnson, J. Chem. Phys. **69**, 4678 (1978).

[67] L. M. C. Janssen, G. C. Groenenboom, A. van der Avoird, P. S. Żuchowski, and R. Podeszwa, J. Chem. Phys. **131**, 224314 (2009).

[68] M. Przybytek and B. Jeziorski, Chem. Phys. **401**, 170 (2012).

[69] A. Dalgarno and R. McCarroll, Proc. R. Soc. London A **237**, 383 (1956).

[70] I. Angeli and K. P. Marinova, At. Data Nucl. Data Tables **99**, 69 (2011).

[71] R. Moszyński, G. Łach, M. Jaszuński, and B. Bussery-Honvault, Phys. Rev. A **68**, 052706 (2003).

[72] R. J. Le Roy, in *Molecular Spectroscopy, Specialist Periodical Reports*, Vol. 1 (The Chemical Society, London, 1973), pp. 113–176.

[73] M. Przybytek, W. Cencek, B. Jeziorski, and K. Szalewicz, Phys. Rev. Lett. **119**, 123401 (2017).

[74] J. S. Coursey, D. J. Schwab, J. J. Tsai, and R. A. Dragoset, Atomic Weights and Isotopic Compositions (version 4.1), Tech. Rep., National Institute of Standards and Technology, Gaithersburg, MD, 2017.

[75] M. S. Safronova, S. G. Porsev, and C. W. Clark, Phys. Rev. Lett. **109**, 230802 (2012).

[76] S. G. Porsev, M. S. Safronova, A. Derevianko, and C. W. Clark, Phys. Rev. A **89**, 012711 (2014).

[77] K. Enomoto, M. Kitagawa, K. Kasa, S. Tojo, and Y. Takahashi, Phys. Rev. Lett. **98**, 203201 (2007).

[78] T. Fukuhara, S. Sugawa, Y. Takasu, and Y. Takahashi, Phys. Rev. A **79**, 021601(R) (2009).

[79] R. J. Le Roy and R. B. Bernstein, J. Chem. Phys. **52**, 3869 (1970).

[80] E. Clementi, D. L. Raimondi, and W. P. Reinhardt, J. Chem. Phys. **471**, 1300 (1967).

[81] M. Borkowski, A. A. Buchachenko, R. Ciuryło, P. S. Julienne, H. Yamada, K. Yuu, K. Takahashi, Y. Takasu, and Y. Takahashi, J. Phys. Conf. Ser. **810**, 012014 (2017).